Polaronic WO_4^{3-} centres in $PbWO_4$ single crystals

1998 J. Phys.: Condens. Matter 10 7293

(http://iopscience.iop.org/0953-8984/10/32/020)

J. Phys.: Condens. Matter **10** (1998) 7293–7302. Printed in the UK PII: S0953-8984(98)92719-9

Polaronic WO_4^{3-} centres in $PbWO_4$ single crystals

V V Laguta†, J Rosa‡‖, M I Zaritskii‡, M Nikl‡ and Y Usuki§

† Institute for Problems of Material Sciences, Krgiganovskogo 3, 252180 Kiev, Ukraine
‡ Institute of Physics, Academy of Sciences of the Czech Republic, Division of Solid State Physics, Cukrovarnicka 162 53 Prague 6, Czech Republic
§ Furukawa Company, Kamiyoshima, Yoshima, Iwaki 970-11, Japan

Abstract. The autolocalization of free electrons at $PbWO_4$ regular lattice sites, namely at WO_4^{2-} complex anions, has been demonstrated by ESR measurements. It has been shown that the WO_4^{3-} centre is a shallow donor; its energy level is situated ≈50 meV below the bottom of the $PbWO_4$ conduction band. At temperatures of 50–60 K the captured electrons are detrapped and the formation of other paramagnetic centres occurs. In La-doped $PbWO_4$, an enhanced cross-section for electron trapping by MoO_4^{2-} impurity centres with respect to that for undoped samples is found. In contrast to the case for other tungstates, no intrinsic oxygen hole and/or Pb^{3+} centres were revealed in $PbWO_4$. The role of the WO_4^{3-} centres in the processes of transport and recombination of nonequilibrium carriers in the $PbWO_4$ lattice is discussed.

1. Introduction

Lead tungstate—$PbWO_4$ (PWO)—has become a very intensively studied material during recent years due to its potential application as a new scintillation material in calorimetric detectors of high-energy-physics accelerators [1–3]. Optical investigations have shown that PWO is characterized by a complex behaviour of emission properties [4, 5], the influence of trapping centres on the decay kinetics [6], optical transmission spectra, as well as radiation damage [7]. In attempts to provide an explanation of the nature and properties of optical absorption spectra before and after irradiation, several mechanisms have been suggested, based on the capture of free charge carriers at intrinsic point defects (e.g. a hole O^- colour centre [8], an F, F^+ centre [9], and a Pb^{3+} centre [10, 11]). The existence of a Pb^{3+} centre might be expected because of its rather stable appearance in the isostructural $CaWO_4$ lattice [12]. Most of these models are based on the assumption of electroneutrality of the crystal, and on the existence of similar centres in other tungstates and oxides. Such a hypothesis should be verified by means of a method providing a sensitive tool for monitoring unpaired spins of electrons/holes captured at such colour centres, e.g. by electron spin-resonance (ESR) measurements. In this way, a detailed theoretical calculation of the electron centre structure and its stability can also be performed.

Radiation-induced colour centres have been extensively studied and well described for many others tungstates, such as $CaWO_4$, $BaWO_4$, $SrWO_4$, and $MgWO_4$. In these materials WO_4^{3-} centres are created mostly after γ- or x-ray irradiation [13]. They are formed by the capture of an electron by the WO_4^{2-} complex perturbed by another defect at the neighbour cation site. Such a WO_4^{3-} centre is stable up to room temperature. Another intrinsic defect studied in the tungstates is the oxygen-related hole centre $(WO_4)_2^{3-}$ [14]. The structure of both of these types of defect was studied by means of ESR in detail.

‖ Author to whom any correspondence should be addressed; e-mail: rosa@fzu.cz.

0953-8984/98/327293+10$19.50

Paramagnetic defects in lead tungstate have not been much investigated up to now. Only the MoO_4^{3-} centre was reported [15], which is created by x-ray irradiation at liquid nitrogen temperature. Gd^{3+} centres were characterized by ESR measurements [16], and also a study of Ce^{3+} and Nd^{3+} ESR spectra in PWO single crystals was performed by two of us in reference [17].

In the present article, we have carried out a study of ESR spectra of nominally pure and La-doped high-quality $PbWO_4$ single crystals after UV irradiation at liquid helium temperature. We have found a new, intensive ESR spectrum, ascribed to intrinsic WO_4^{3-} defects. In contrast to the case for other tungstates, this defect is created by autolocalization of an electron near a regular W^{6+} site. The region of temperature stability of the centre and the position of its electronic level were determined. The role of the WO_4^{3-} centres in the processes of transport and recombination of nonequilibrium carriers in the $PbWO_4$ lattice is discussed.

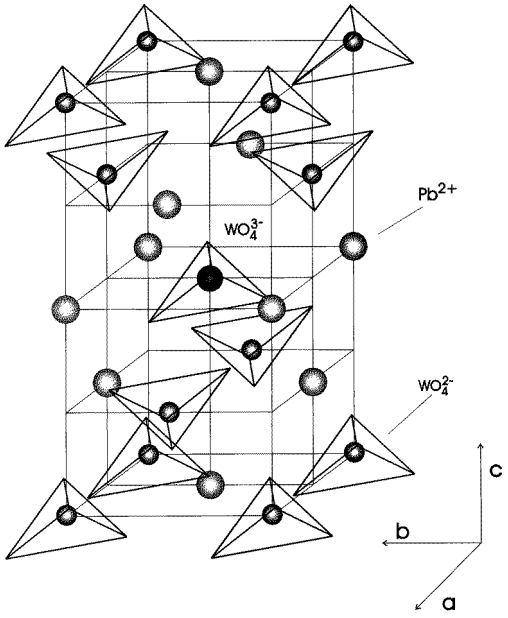

Figure 1. The unit cell of $PbWO_4$ crystal having scheelite structure.

2. Experimental procedure

The unit cell of the scheelite PWO structure is illustrated in figure 1; its space group is C_{4h}^6, and the main crystallographic parameters can be found, e.g., in reference [18].

For most of the experiments, we used undoped (No 1) and La-doped (No 2) PWO single crystals grown by the Czochralski method in air in the third crystallization [19]. GDMS (glow discharge mass spectroscopy) analysis was performed, and this showed that any unwanted impurities were at a level below 1 ppm. The La concentration was about 200 molar ppm in sample No 2. To determine the Mo concentration, ICP (inductively coupled plasma) analysis was performed as well, showing the Mo concentrations in both of the samples to be at a level below 0.5 ppm. Oriented (using x-ray diffraction with a precision

of $\pm 0.5^\circ$) parallelepiped-shaped samples, $2.4 \times 2.6 \times 5$ mm^3, were cut in (001) and (100) planes.

The ESR measurements were performed at 9.21 GHz in the standard 3 cm wavelength range of an ESR spectrometer at temperatures of 4–300 K. An Oxford Instruments ESR-9 cryosystem was used. The applied magnetic field was rotated in the (001) and (100) planes of the PWO crystal structure.

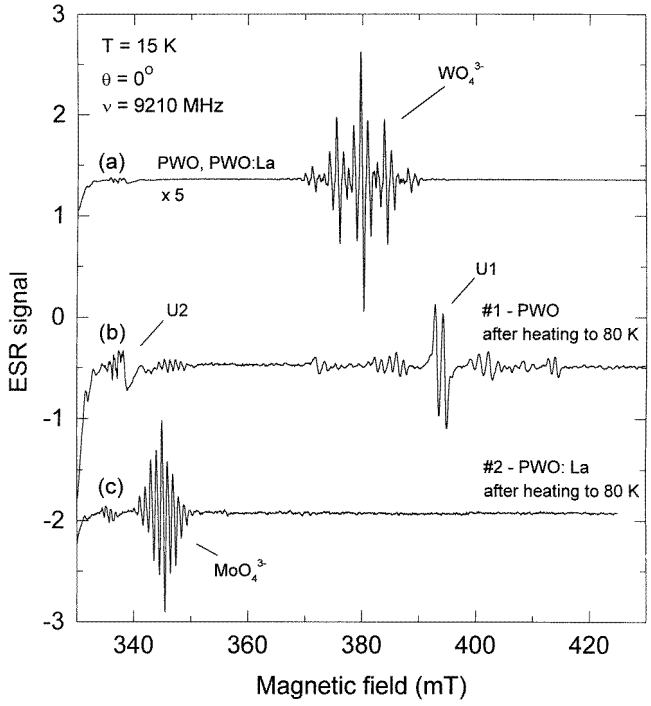

Figure 2. ESR spectra of light-induced centres in $PbWO_4$; (a) WO_4^{3-}; the signal should be multiplied by a factor of 5 for absolute comparison with the other two curves; (b) groups of resonant lines U1, U2 of unknown defects; (c) MoO_4^{3-}.

3. Experimental results

3.1. ESR spectra

Only weak-intensity spectra of Ce^{3+} and Nd^{3+} were observed for both of the samples, No 1 and No 2, before illumination, in agreement with the results of reference [17]. After illumination of the samples with UV light of $\lambda \cong 260$–330 nm at $T < 50$ K, a new intense ESR spectrum with well resolved superhyperfine structure appears (see figure 2(a)). Such a spectrum was generated for both samples with approximately equal intensity. The spectrum is found to be very anisotropic, but with exactly axial symmetry about the crystal c-axis. The resonance fields of the central component of the superhyperfine structure have been described by a spin Hamiltonian for paramagnetic ions with $S = 1/2$ and g-factor values of $g_\parallel = 1.733(1)$, $g_\perp = 1.476(1)$, where the subscript $\parallel$ corresponds to the tetragonal c-axis direction (see figure 1). As has been shown by detailed analysis, the ESR spectrum consists

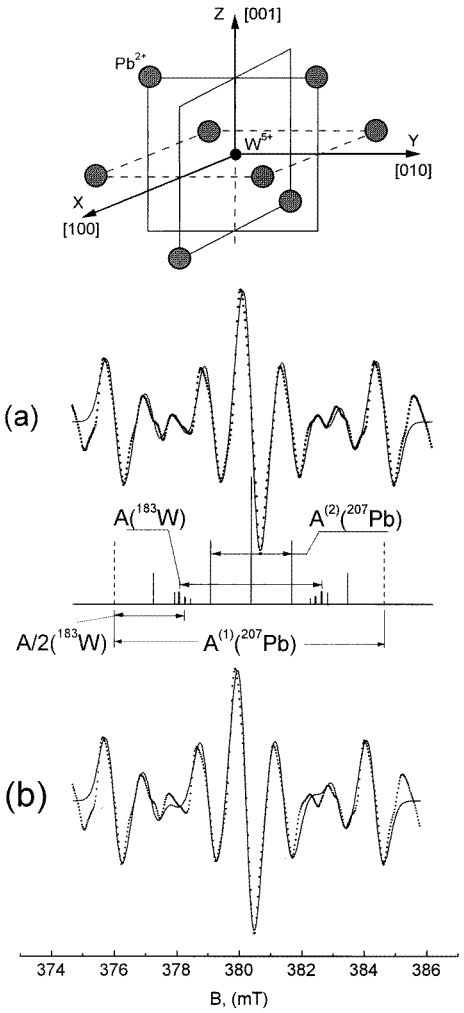

Figure 3. The central part of the ESR spectrum of the WO_4^{3-} centre for $\boldsymbol{B} \parallel [001]$ with computer simulation of both ^{207}Pb and ^{183}W (super)hyperfine structures (a) and with ^{207}Pb superhyperfine structure only (b). The experimental and calculated data are represented by dots and solid lines, respectively. We schematically show a pattern of ^{207}Pb and ^{183}W (super)hyperfine splittings, which have been included in the simulations. $A^{(1)}(^{207}\mathrm{Pb})$ and $A^{(2)}(^{207}\mathrm{Pb})$ are shf splittings, arising from two groups of ^{207}Pb nuclei arranged in square-planar and D_{2d} symmetry, respectively. The small degree of asymmetry of the experimental lines originates from the second-order hf splitting, which was not taken into account.

of hyperfine (hf) and superhyperfine (shf) structures, the latter originating from two groups of ^{207}Pb nuclei.

The strongest superhyperfine interaction was described by the hyperfine tensor with weak [110] axiality, $|A_{\parallel}^{(1)}| = 61(1) \times 10^{-4}$ cm^{-1} and $|A_{\perp}^{(1)}| = 70(1) \times 10^{-4}$ cm^{-1}. For $\boldsymbol{B} \parallel [001]$, it splits the ESR line into seven, easily identified components with the ratio of integral intensities 1:10:48:100:48:10:1. Such a pattern can arise due to the interaction of a paramagnetic ion at a W^{6+} site with four equivalent ^{207}Pb nuclei ($I = 1/2$; natural abundance 22.6%), which are arranged around the tungsten ion in a square-planar symmetry

(see figure 3). In such a case, the ratio of superhyperfine-line intensities was calculated as 0.9:9.8:48.4:100:48.4:9.8:0.9. The second superhyperfine interaction, of lower amplitude, splits each of these seven lines into other well resolved components with the observed ratio of integral intensities 10:48:100:48:10. This can be ascribed again to the interaction of a paramagnetic ion with four D_{2d}-arranged ^{207}Pb nuclei, far from the paramagnetic ion in this case. The hyperfine tensor, which describes this interaction, shows axial symmetry along the [011] and [101] directions, $|A_{\parallel}^{(2)}| = 15(1) \times 10^{-4}$ cm^{-1} and $|A_{\perp}^{(2)}| = 26(1) \times 10^{-4}$ cm^{-1}. Because of the smaller splitting, we cannot resolve the lowest (1%) intensity lines, as we could for the first set.

In addition to the above-mentioned groups of shf lines, low-intensity hyperfine lines can also be observed, which we ascribe to the ^{183}W nucleus ($I = 1/2$; natural abundance 14.4%). These lines are visible in orientations of $\boldsymbol{B}$ close to [001] when the shf splittings from the ^{207}Pb nuclei within each of the groups are the most nearly equivalent (figures 2(a) and 3(a)). It is very difficult to separate them for the other directions of the external magnetic field due to their small intensity ($\approx$8%) and overlap with intense ^{207}Pb shf lines. Moreover, ^{207}Pb nuclei become inequivalently oriented, which leads to additional splitting of their lines. For $\boldsymbol{B} \parallel$ [001], we have carried out a computer simulation of the central part of the spectrum where the hf lines from the ^{183}W isotope are the most intense. Thus we have determined the ^{183}W hf splitting $A(^{183}\mathrm{W}) = 34(1) \times 10^{-4}$ cm^{-1} as well as the relative intensity of the lines (8.5%), the latter being in good agreement with the expected value. The necessity of including ^{183}W hf lines in the spectrum simulation is evident in figure 3—see curves (a) (hf lines included) and (b) (hf lines not included).

On the basis of the above-mentioned data we can assume that the spectrum of figure 2 relates to the paramagnetic ion W^{5+} (a WO_4^{3-} centre) which was created by an electron trapped by the WO_4^{2-} complex anion. Such a model is supported by the following additional arguments.

The superhyperfine interaction of the electron with two groups of ^{207}Pb nuclei shows that the W site is its position of localization. In the $PbWO_4$ crystal structure a W^{6+} ion is surrounded by four Pb^{2+} ions (in the *ab*-plane at a distance of 0.3888 nm). The next four Pb^{2+} ions occupy the positions in the *ac*-planes, or *bc*-planes, separated by distances of 0.4092 nm (see figures 1 and 3). Such topography of Pb^{2+} ions exactly corresponds to the observed superhyperfine structure of ESR spectra as well as to the symmetry of hyperfine tensors. Moreover, the g-factor shift is typical of a $5d^1$-electron configuration in a crystal-field potential created by four D_{2d}-arranged oxygen ions. The experimentally observed g- and A-tensors clearly indicate that the ground orbital state of the centre has to be d_{z^2} [20]. In such a case, $\Delta g_{\parallel} = g_{\parallel} - g_e = 0$ and $\Delta g_{\perp} = g_{\perp} - g_e = -3g_e\lambda_{eff}/\Delta$, where g_e is the g-factor of a free electron, λ_{eff} represents the reduced spin–orbit coupling constant, and Δ is the energy gap between the ground and the nearest excited state. Such a model can explain the relation $g_{\parallel} > g_{\perp}$. However, it is not able to explain the large $g_{\parallel}$-shift $\Delta g_{\parallel} = -0.27$. So, like the authors of reference [15], we can conclude that the large deviation from the free-electron value is due to the large covalency contribution from the first shells of four neighbouring lead cations. This conclusion is also confirmed by the anomalously strong hyperfine interaction of the electron with the ^{207}Pb nuclei.

Comparison of our results (the g-factor and ^{207}Pb shf matrix) for the WO_4^{3-} and MoO_4^{3-} centres, studied in [15] and observed by us in some samples after heating them up to 80 K (see figure 2), indicates very similar spectral characteristics of these centres. That is why we do not carry out any detailed analysis of the g- and A-values for WO_4^{3-}. Such an analysis was done in the framework of a covalent model of the electron MoO_4^{3-} centre and

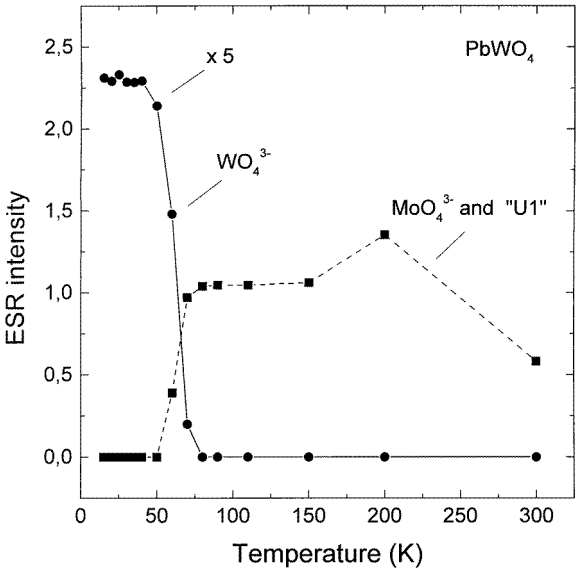

Figure 4. The temperature dependence of the ESR intensity of the light-induced centres, determined by isochronal annealing.

is acceptable for the centre WO_4^{3-} as well. Therefore, our attention was mainly confined to the study of the temperature stability and the nature of this defect.

3.2. The thermal stability and energy levels of the WO_4^{3-} centre

The thermal stability of the centre was studied by the method of isochronal annealing; the sample was heated to a given temperature, held at that temperature for one minute, and quickly cooled down to 14–15 K, whereupon the ESR spectrum was measured. The signal amplitudes obtained are depicted in figure 4. It can be seen that the WO_4^{3-} centres are rather shallow, as the spectrum disappears after the heating of the sample to 50–55 K. Then new spectra are observed (see figure 2(b) and 2(c)) indicating recapture of electrons at other lattice positions. For sample No 2, this new spectrum relates to the MoO_4^{3-} centre. For sample No 1 we have obtained two new, not previously observed spectra of orthorhombic symmetry marked as 'U1' and 'U2' in figure 2(b). These spectra, as well as the spectrum of MoO_4^{3-}, are stable up to temperatures of 270–280 K.

From the fact that the WO_4^{3-} centres are thermally ionized at low temperatures, we can conclude that their energy level is positioned close to the bottom of the conduction band (which is constructed mainly from the d states of W atoms). The thermal ionization energy was obtained from the measurements of the ionization probability expressed in the form of an Arrhenius law: $P(T) = N_e S v \exp(-E_a/kT)$ (see, e.g., reference [21]). (N_e is the effective density of states in the conduction band; v and S are the electron thermal velocity and cross-section of its capture, respectively, and E_a stands for thermal ionization energy.) The value of P at any temperature can be obtained from the measurement of the time decay of the localized carrier concentration after switching off the light. If one neglects the possibility of carrier recapture (creating the same centre again), the decay of the concentration of the localized electrons can be described by an exponential time dependence,

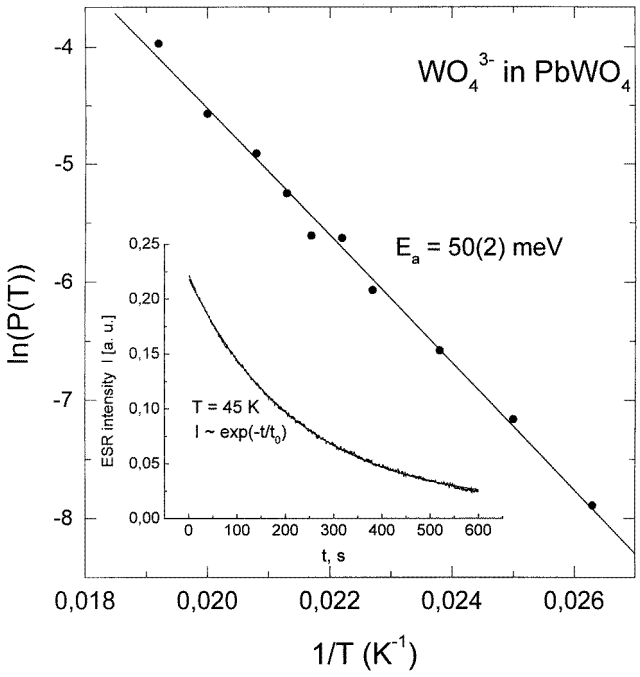

Figure 5. The temperature dependence of the thermal ionization probability of the WO_4^{3-} centre.

$n = n_0 \exp(-P(T)t)$, which was actually observed in our experiments (see figure 5).

The product $N_e S v$ can be estimated to be at most proportional to T^2. Therefore, it is mainly the exponent that determines the temperature dependence of the centre's ionization probability $P(T)$. The results of the experimental data analysis are plotted in figure 5 where the slope of the line gives the energy of the thermal ionization of the centre.

4. Discussion

According to the position of the UV edge of the thermally stimulated luminescence (TSL) excitation spectra at low temperatures [22], illumination of PWO using a wavelength of around 260 nm will result in the creation of uncorrelated electron–hole pairs, which may become localized at separate lattice sites. As the observed paramagnetic WO_4^{3-} centre is an intrinsic centre, not impurity related, in the PWO lattice, it is very important to understand the mechanism of its creation. It was mentioned earlier that the tungsten ion can give rise to a local energy level in the forbidden gap under the condition that there is another defect in its neighbourhood. The WO_4^{3-} centres observed earlier in other tungstates (see, e.g., [13]) usually showed lower symmetry than that of the regular W site and thermal stability up to room temperature. This was explained by the existence of some impurity ion at a neighbouring Pb site.

The WO_4^{3-} centre in PWO shows tetragonal symmetry and thermal stability only up to approximately 50 K. The high symmetry of WO_4^{3-} suggests that there is no vacancy or impurity ion nearby; otherwise the symmetry would be lower. The only exception might be for a Pb site lying on the *c*-axis passing through the W site. On the other hand, such a position is too far from the paramagnetic ion to make a significant contribution. Furthermore,

the concentration of WO_4^{3-} centres differs only weakly in all of the samples studied and can be estimated to be around 5–10 at. ppm. According to the chemical analyses mentioned above, there is no impurity with such a high concentration in these crystals. Hence, the observed WO_4^{3-} centre is created as a result of autolocalization of an electron at the regular lattice site of the W^{6+} ion, i.e. WO_4^{3-} can be described as a small-radius polaron [23]. Such a centre usually has a low ionization energy—in our case not exceeding 0.05 eV—and its wave function is rather widely spread, like that of the F centre. The observed strong superhyperfine interaction and the big shift of the g-factor are the results of overlap of the wave function of the autolocalized electron with atomic orbitals of neighbouring cations. Furthermore, the magnitude of the ^{183}W hf splitting is smaller in comparison with that for a thermally more stable defect-related WO_4^{3-} centre in other tungstates, which is also evidence of the partial delocalization of unpaired electrons. In general, autolocalization of an electron at a regular lattice site has already been observed in some crystals. For instance, evidence of an isolated Ti^{3+} centre in $BaTiO_3$ was reported in [24].

If polarons occur, they automatically have a marked effect on the electron transport through the localization of the free electrons in the crystal lattice. As they are created at regular lattice sites, such mechanisms are important in very pure crystals in which the probability of free-carrier trapping by an impurity becomes very low. Even at higher temperatures, trapping and detrapping processes related to polaronic states might influence the characteristic recombination time (second order), the decay components in the photoluminescence, and the scintillation mechanisms. In PWO, the coexistence of first- and second-order decay kinetics was proved by means of TSL and photoluminescence experiments at room temperature [6].

Detrapping of electrons at around 50–60 K can also explain the TSL peaks observed in this temperature region [25]. As the related TSL spectrum is situated mainly in the blue spectral region, where the emission component related to the regular lattice site (WO_4^2) occurs, opposite charge carriers (holes) must be still localized at another (regular) lattice site at these temperatures. These hole centres thus capture diffusing electrons, and radiative recombination occurs at regular lattice sites giving rise to the blue emission component. In fact, Pb^{3+} and O^- hole centres were proposed as possible hole-centre configurations to explain absorption features for $E \leqslant 3.7$ eV in as-grown and/or irradiated PWO [10, 11]. In contrast to the case for the other tungstates, however, no intrinsic oxygen hole centres were observed in the PWO single crystals, and no Pb^{3+} centres similar to those in $CaWO_4$ [12] were found during the present ESR experiments either. This may be connected with the fact that in PWO and $PbMoO_4$ [26], as well as in other oxygen crystals with lead cations, the top of the valence band is formed to a considerable extent by the 6s states of Pb and not only by 2p oxygen orbitals. Thus rather a mixed Pb–O character of intrinsic hole centres in these compounds can be expected. As an example, in $PbTiO_3$, Ti^{3+}–V_0 donor centres can be easily found [27], but O^- hole centres are not observed, in contrast to the case for $BaTiO_3$, in which both types of defect can be realized [24, 28].

Another interesting effect consists in the apparently different intensity of the ESR signal of MoO_4^{3-} centres in the illuminated samples No 1 and No 2 after heating up to 80 K. Even if there is no precise determination of the Mo content in these samples (the Mo concentration is close to the detection limit for ICP), it is very probable that the Mo contamination is on a comparable level in the two samples (the same raw material and growth procedure). Then, a possible explanation consists in the enhancement of the electron capture cross-section of MoO_4^{2-} electron traps due to local Coulombic potential variation induced by an excess charge of La^{3+} ions at Pb sites. The enhanced radiation resistance of La-doped crystals [29] was explained by a decrease of the stable and temporary hole-centre concentrations in the

PWO lattice, occurring because of the excess positive charge introduced by La^{3+} doping into the Pb sublattice. Hence, in regions of the crystal containing La ions, hole centres are destabilized, while enhanced stability of electron trapping centres can be expected, resulting in an enhanced cross-section for electron capture. Alternatively, lack of competing processes for electron capture in La-doped samples could explain the enhanced occurrence of MoO_4^{3-} centres at 80 K as well.

In conclusion, autolocalization of electrons in the regular PWO lattice at the WO_4^{2-} complex anion has been observed below 60 K. To explain earlier-reported TSL characteristics for this temperature region [25], hole autolocalization has to occur as well, even though the related ESR spectra have not shown the simple Pb^{3+} and/or O^- hole centres that were considered until now to be the most logical choice.

Acknowledgments

The authors are grateful for the financial support of the grant AV CR A1010714, and to A Vedda for useful discussions.

References

[1] Kobayashi M, Ishii M, Usuki I and Yahagi M 1993 *Nucl. Instrum. Methods Phys. Res.* A **333** 429
[2] Lecoq P, Dafinei I, Auffray E, Schneegans M, Korzhik M V, Missevitch O V, Pavlenko V B, Fedorov A A, Anenkov A N and Kostylev V L 1995 *Nucl. Instrum. Methods Phys. Res.* A **365** 291
[3] Zhu R Y, Ma D A, Newman H B, Woody C L, Kirstead J A, Stoll S P and Levy P W 1996 *Nucl. Instrum. Methods* A **376** 319
[4] Nikl M, Nitsch K, Polak K, Mihokova E, Dafinei I, Auffray E, Lecoq P, Reiche P, Uecker R and Pazzi G P 1996 *Phys. Status Solidi* b **195** 311
[5] Tamulaitis G, Buracas S, Martinov V P, Ryzhikov V D, Gutbrod H H and Manko V I 1996 *Phys. Status Solidi* a **157** 187
[6] Martini M, Spinolo G, Vedda A, Nikl M, Nitsch K, Hamplova V, Fabeni P, Pazzi G P, Dafinei I and Lecoq P 1996 *Chem. Phys. Lett.* **260** 418
[7] Auffray E, Dafinei I, Gantheron F, Lafond-Puyet O, Lecoq P and Schneegans M 1996 *Proc. Int. Conf. SCINT95—Inorganic Scintillators and Their Applications* (Delft: Delft University Press) pp 282–5
[8] Nikl M, Nitsch K, Hybler J, Chval J and Reiche P 1996 *Phys. Status Solidi* b **196** K7
[9] Nikl M, Rosa J, Nitsch K, Asatryan H R, Baccaro S, Cecilia A, Montecchi M, Borgia B, Dafinei I, Diemoz M and Lecoq P 1997 *Mater. Sci. Forum* **239–241** 271
[10] Nikl M, Nitsch K, Baccaro S, Cecilia A, Montecchi M, Borgia B, Dafinei I, Diemoz M, Martini M, Rosetta E, Spinolo G, Vedda A, Kobayashi M, Ishii M, Usuki J, Jarolimek O and Reiche P 1997 *J. Appl. Phys.* **82** 5758
[11] Anenkov A N, Fedorov A A, Galez P, Katchanov V A, Korzhik M V, Ligun V D, Moreau J M, Nefedov V N, Pavlenko V B, Peigneux J P, Timoshenko T N and Zadneprovskii B A 1996 *Phys. Status Solidi* a **156** 493
[12] Born G, Hofstaetter A and Scharmann A 1970 *Phys. Status Solidi* **37** 255
[13] Solntsev V P and Shcherbakova M V 1971 *Proc. Conf. on Magnetic Resonance and Related Phenomena (Bucharest)* (Bucharest: The Academy of Romania) p 937
[14] Born G, Grasser R and Scharmann A 1968 *Phys. Status Solidi* **28** 583
[15] Hofstaetter A, Scharmann A, Schwabe D and Vitt B 1978 *Z. Phys.* B **30** 3055
[16] Meilman M L 1966 *Fiz. Tverd. Tela* **8** 3656
[17] Rosa J, Asatryan H R and Nikl M 1996 *Phys. Status Solidi* a **158** 573
[18] Wyckoff R W G 1951 *Crystal Structures* vols 2, 8 (New York: Interscience)
[19] Kobayashi M, Ishii M, Harada K, Usuki Y, Okuno H, Shimizu H and Yazawa T 1996 *Nucl. Instrum. Methods* A **373** 333
[20] Abraham A and Bleaney B 1970 *Electron Paramagnetic Resonance of Transition Ions* (Oxford: Clarendon)
[21] Bube R 1960 *Photoconductivity of Solids* (New York: Wiley)
[22] Murk V, Nikl M, Mihokova E and Nitsch K 1997 *J. Phys.: Condens. Matter* **9** 249

[23] Pekar S I 1958 *Sov. Phys.–JETP* **6** 785 (in Russian)
Pekar S I 1958 *Sov. Phys.–JETP* **7** 813 (in Russian)
[24] Scharfschwerdt R, Mazur A, Schirmer O F, Hesse H and Mendricks S 1996 *Phys. Rev.* B **54** 15 284
[25] Springis M, Tale V and Tāle I 1997 *J. Lumin.* **72–74** 784
[26] Zhang Y, Holzwarth N A W and Williams R T 1998 *Phys. Rev.* B **57** 12 738
[27] Laguta V V, Glinchuk M D, Bykov J P, Maksimenko Yu L, Rosa J and Jastrabik L 1996 *Phys. Rev.* B **54** 12 353
[28] Varnhorst T, Schirmer O F, Kröse H, Scharfschwerdt R and Kool Th W 1996 *Phys. Rev.* B **53** 116
[29] Baccaro S, Bohácek P, Borgia B, Cecilia A, Dafinei I, Diemoz M, Ishii M, Jarolimek O, Kobayashi M, Martini M, Montecchi M, Nikl M, Nitsch K, Usuki Y and Vedda A 1997 *Phys. Status Solidi* a **160** R5